Journal of Applied Physics

RESEARCH ARTICLE | APRIL 24 2023

Microstructure enhancement of macroscopic flexoelectric behavior of THV/Al composites

Ju Hwan (Jay) Shin; Mikel J. Zaitzeff; Lori J. Groven; ... et. al

Check for updates

Journal of Applied Physics 133, 164101 (2023)
https://doi.org/10.1063/5.0141173

View Online
Export Citation
CrossMark

Articles You May Be Interested In

Multi-functional electroactive tetrafluoroethylene-hexafluoropropylene-vinylidene fluoride (THV)/magnesium diboride (MgB_2) composite reactive material

Journal of Applied Physics (February 2023)

Shock compression response of alumina-THV composites

Journal of Applied Physics (January 2011)

Equation of state and high pressure properties of a fluorinated terpolymer: THV 500

Journal of Applied Physics (December 2008)

Downloaded from http://pubs.aip.org/aip/jap/article-pdf/doi/10.1063/5.0141173/16966722/164101_1_5.0141173.pdf

AIP Publishing

Journal of Applied Physics ARTICLE scitation.org/journal/jap

Microstructure enhancement of macroscopic flexoelectric behavior of THV/Al composites

Cite as: J. Appl. Phys. **133**, 164101 (2023); doi: 10.1063/5.0141173
Submitted: 3 January 2023 · Accepted: 12 April 2023 ·
Published Online: 24 April 2023

View Online Export Citation CrossMark

Ju Hwan (Jay) Shin,[1] Mikel J. Zaitzeff,[2] Lori J. Groven,[2] and Min Zhou[1,a)]

AFFILIATIONS

[1]The Woodruff School of Mechanical Engineering, School of Materials Science and Engineering, Georgia Institute of Technology, Atlanta, Georgia 30332, USA
[2]Karen M. Swindler Department of Chemical and Biological Engineering, South Dakota School of Mines and Technology, Rapid City, South Dakota 57701, USA

[a)]**Author to whom correspondence should be addressed:** min.zhou@gatech.edu. **Telephone:** 404-894-3294. **Fax:** 404-894-8336.

ABSTRACT

Flexoelectricity is often studied at the macroscopic scale for energy conversion and harvesting. The fact that microstructural heterogeneities can have a profound impact on a material's flexoelectric response has been under-appreciated and largely unexplored. To capture the effects of microstructure on both the macroscopic flexoelectric behavior and the development of microscopic electric field that drives such microscale processes, we develop a computational framework that enables the quantification of how the microstructure can influence the flexoelectric behavior of heterogeneous materials. The specific material evaluated is a porous composite of tetrafluoroethylene-hexafluoropropylene-vinylidene fluoride polymer and aluminum (Al) particles. The models explicitly resolve the Al particles and voids within the microstructure. The focus of the analysis is on assessing the physical mechanisms that enhance the macroscopic flexoelectric output and determining the effective flexoelectric coefficient of the inhomogeneous material. The approach also allows the contributions of individual strain gradient components to the effective flexoelectric coefficient to be delineated and offers a method of determining the flexoelectric coefficients associated with individual strain gradient components using measurements of the macroscopic flexoelectric responses of microstructures with different concentrations of Al particles and voids. It is concluded that the enhancement of local strain gradients near the Al particles and voids and the activation of contributions from multiple strain gradient components are the primary mechanisms for the increase in the macroscopic flexoelectric output of the composites. The macroscopic flexoelectric coefficient under cantilever beam bending is found to rise linearly with the Al content, consistent with the experimental measurements.

Published under an exclusive license by AIP Publishing. https://doi.org/10.1063/5.0141173

I. INTRODUCTION

Flexoelectricity is an electromechanical phenomenon in which strain gradient induces electric polarization (direct flexoelectric effect) and vice versa (converse flexoelectric effect).[1–4] Similar to piezoelectricity, flexoelectricity has applications in energy harvesting, actuation, MEMS devices, and semiconductors,[5–26] all of which take advantage of the direct and converse effects at the macroscopic level. Recently, experiments and analyses demonstrated[27–30] that the underlying microstructure and material heterogeneities can have a significant impact on the apparent flexoelectric output of materials. This raises the question of how materials can be engineered at the microscopic scale to tailor their macroscopic flexoelectric behavior. On the other hand, flexoelectricity is increasingly recognized for its ability to affect the thermodynamic state of materials at small scales. For instance, the presence of high strain gradients near crack tips was shown to substantially influence the fracture behavior.[31] Also, under certain loading conditions, the development of high strain gradients in polymer–metal composites was shown to be responsible for the high electric field (*E*-field) within the inhomogeneous material, ultimately leading to dielectric breakdown. Such events can cause localized heating (also referred to as "hotspots") that results in the onset of chemical reactions[32–35] in energetic materials (EMs). This leads to an exciting means for precisely controlling the ignition behavior of EMs or devices using such materials. Many of these events can occur even under conditions dominated by microscopic strain gradients but involve low or no net strain gradients at the macroscopic level. Such microscopic flexoelectric effects remain underexplored.

Downloaded from http://pubs.aip.org/aip/jap/article-pdf/doi/10.1063/5.0141173/16966722/164101_1_5.0141173.pdf

Published under an exclusive license by AIP Publishing

Fluoropolymers such as tetrafluoroethylene-hexafluoropropylene-vinylidene fluoride (THV) are flexoelectric. Previous studies mostly focused on the piezoelectric and flexoelectric properties of poly(vinylidene fluoride) (PVDF) and its co- and terpolymers,[18,19,27,32,33,35–38] while the flexoelectric coefficient of a homogeneous (neat) THV polymer has only been reported recently.[28] The flexoelectric response of inhomogeneous THV or other flexoelectric materials at the macroscopic level is much less understood. This poses a challenge in the development of materials with enhanced flexoelectric properties via microstructural engineering for a variety of materials.

The intentional introduction of heterogeneities through composite formation has been shown to offer a route to enhance both the piezoelectric and flexoelectric properties of polymers via microstructure modification while maintaining their mechanical integrity.[37–41] For example, the addition of piezoelectric ceramic inclusions, such as lead zirconate titanate (PZT) into PVDF, can result in overall piezoelectric coefficients as high as 40 pC/N (~2 times higher than those of neat PVDF).[39,40] The electroactive characteristics of microstructures can also be enhanced via changes in porosity. By increasing the porosity level of a PVDF thin film, the piezoelectric output was observed to increase by as much as 100%.[42] On the other hand, porosity was also shown to play a role in influencing flexoelectricity.[43,44] For instance, Zhang[43] reported an ultrahigh flexoelectric effect for porous polydimethylsiloxane and PVDF. While the piezoelectric effect of composite materials is reasonably well understood, there is growing interest in further elucidating the influence of microstructural design on flexoelectricity for all material types. Recently, Zaitzeff and Groven determined experimentally[28] that the effective (i.e., macroscopic) flexoelectric coefficient of THV/Al composites increases linearly with the weight fraction (η_{Al}) of embedded aluminum (Al) particles (e.g., up to 53% increase in an aluminized composite compared to a homogeneous THV polymer). This finding highlights the need to study the mechanism through which this effect occurs and quantify the influence that the underlying microstructure has on the electromechanical behavior.

We present a novel computational framework for analyzing the effects of microstructural heterogeneities, such as embedded voids and Al particles, on the electromechanical behavior of the materials at both the microscopic and macroscopic (or structural) levels. A set of statistically similar microstructure models are generated and used to analyze the deformation and flexoelectric response of the THV/Al composites under cantilever beam bending (CBB).[45–47] Furthermore, a systematic method is developed in order to numerically predict the effective flexoelectric coefficient ($\bar{\mu}^{\circ}_{TR}$) of the composites as a function of the transverse, shear, and longitudinal strain gradients. The predicted values of the effective flexoelectric coefficient are in good agreement with the experimental results.[28] This approach lends itself to applications for other material systems as well.

II. COMPUTATIONAL MODEL AND SIMULATION

A. Microstructure model generation

The microstructures (MSs) of the THV/Al composite comprise Al particles and voids embedded within a THV binder. Both the particles and voids are circular in shape. The Al particles have a weight fraction ranging between 0% and 40% and a Gaussian distribution of diameter with a mean of 3.5 μm and a standard deviation of 0.3 μm. The void diameter is ~25 μm, as shown in Figs. 1(a) and 1(b). The two-dimensional microstructure model [Fig. 1(c)] captures the salient characteristics of the particles and voids. Moreover, the overall size of the model is 100 μm (thickness) × 500 μm (length), as shown in Fig. 2.

To capture and quantify the stochastic nature of the microstructural heterogeneities, a total of 35 sets of non-porous ($\eta_{void} = 0\%$) and porous ($\eta_{void} = 5\%$ and 10%) THV/Al specimens are randomly generated with Al particle weight fractions ranging between 0% and 40% and with different particle sizes ($D_{Al} = 3.5\,\mu$m, 7.0 μm, and 10.5 μm). As an example, the five sets of porous specimens ($\eta_{void} = 10\%$) with a mean particle size of 3.5 μm are illustrated in Fig. 2. Each of the statistically equivalent microstructure sample set (SEMSS) consists of five random but statistically similar specimens. Assessing multiple specimens from the SEMSS allows for a more realistic characterization of the material response, as the analysis yields a range of behavior outcomes based on the random microstructure instantiations. In addition to the SEMSS shown in Fig. 2, the remaining 30 microstructure sets are not shown here for brevity. These additional sets are used to analyze the effects of varying the particle size (3.5, 7.0, and 10.5 μm; no voids; 0%, 10%, 20%, 30%, and 40% particles by weight), void size (10, 25, and 40 μm; 10% porosity; 3.5 μm in particle size; 0%, 10%, 20%, 30%, and 40% particles by weight), and porosity level (0%, 5%, and 10%; 3.5 μm in particle size; 0%, 10%, 20%, 30%, and 40% particles by weight). Together, these SEMSSs enable a systematic study of the effects of different microstructure attributes on the effective flexoelectric output of the specimens.

B. Boundary conditions

The impact-induced electromechanical response of the THV/Al composite from its piezoelectric and flexoelectric properties and subsequently the dielectric breakdown and chemical reaction processes preceding the ignition event are simulated using COMSOL v6.0. Here, the impact loading condition emulates that tested in the experiments,[28] albeit using a smaller specimen. The microstructure is subjected to the cantilever beam bending (CBB) configuration, as illustrated in Fig. 3. The left-hand side of the specimen is fixed such that there is no rotation or displacement. The right-hand side is subjected to an external moment M_0 such that the displacement at the tip of the specimen is $\Delta_0 = 50\,\mu$m in the upward direction. The top and bottom surfaces are traction-free. The specimen is initially stress-free and charge-free. A plane-strain condition is assumed throughout the analysis.

Moreover, the finite element model is discretized into two-dimensional, isoparametric, quadratic Lagrange, triangular elements (with six nodes per element). The average element size in the domain is ~0.6 μm. Among the various sets of microstructures analyzed herein, the maximum number of elements in a given model is ~ 900 000.

C. Governing equations and constitutive relations

The governing equations and constitutive relations for the coupled electromechanical processes are outlined here. A

Downloaded from http://pubs.aip.org/aip/jap/article-pdf/doi/10.1063/5.0141173/16966722/164101_1_5.0141173.pdf

Published under an exclusive license by AIP Publishing

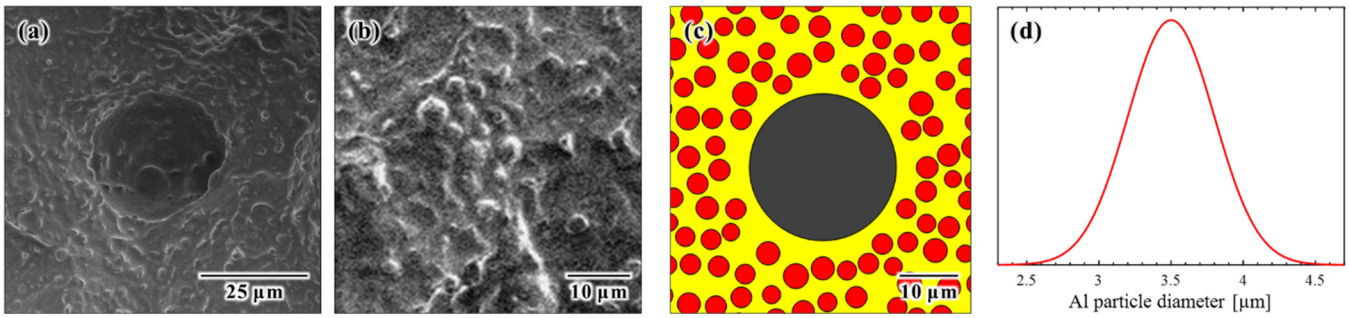

FIG. 1. SEM images showing (a) the voids embedded within the THV polymer and (b) the Al particles; (c) inset view of the microstructure showing Al particles (red) and voids (black) within THV binder (yellow); (d) probability density function of the particle diameters based on a normal Gaussian distribution. For this specimen, mean and standard deviation are 3.5 and 0.3 μm, respectively.

quasistatic model is used, as the load duration is significantly longer than the time needed for the mechanical stress waves to traverse the specimen. A finite deformation formulation is used to account for large deformation and rotation. The mechanical response is governed by the conservation of momentum. On the other hand, the electrostatic response is governed by the conservation of charge (Gauss's law) and Faraday's law of induction applied to quasistatic conditions. In the reference configuration, the equations are

$$\begin{cases} \nabla \cdot (\boldsymbol{FS})^{\mathrm{T}} = \boldsymbol{0}, \\ \nabla \cdot \boldsymbol{D} = \rho_q, \\ \nabla \times \boldsymbol{E} = \boldsymbol{0}, \end{cases} \tag{1}$$

where $\boldsymbol{S}$ and $\boldsymbol{F}$ are the second Piola–Kirchhoff stress and the deformation gradient, respectively. $\boldsymbol{D}$, $\boldsymbol{E}$, and ρ_q represent the electric displacement, the electric field, and the volumetric free-charge density, respectively.

The electric displacement comprises a dielectric polarization part caused by the induced dipole moment and a flexoelectric polarization part caused by the local strain gradients. For large deformation, this electromechanical constitutive relation[48] can be expressed as

$$D_i = \left[\epsilon \delta_{ij} + \epsilon_0 (J F_{ik}^{-1} F_{jk}^{-1} - \delta_{ij})\right] E_j + \mu_{ijkl} \varepsilon_{jk,l}, \tag{2}$$

where $J \equiv \det(\boldsymbol{F})$, E_j, and $\varepsilon_{jk,l} = \partial \varepsilon_{jk} / \partial x_l$ represent the Jacobian, electric field, and the gradient of the Green–Lagrange strain

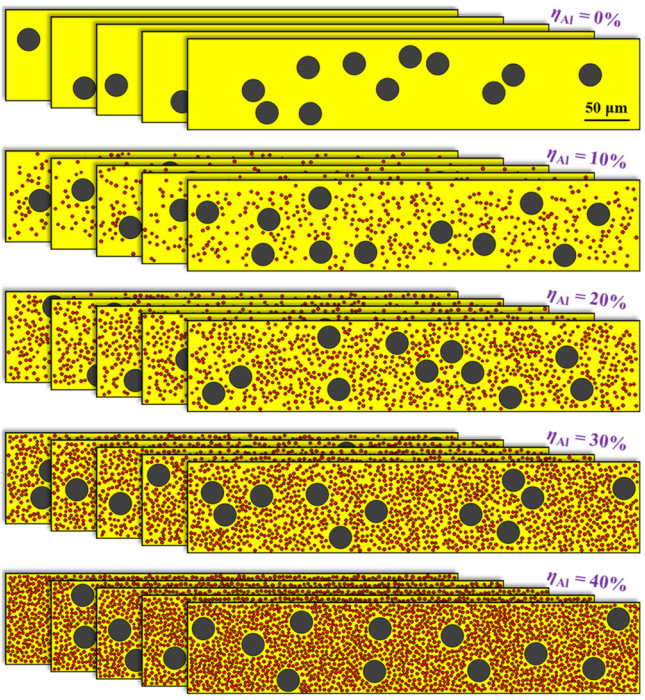

FIG. 2. Statistically equivalent microstructure sample sets (SEMSSs) of THV/Al composites with 10% porosity and void size and mean particle size of 25 and 3.5 μm, respectively. Microstructures shown with varying levels of embedded Al particles (η_{Al}) between 0% and 40% by weight fraction. The overall size of the models is 100 μm (thickness) × 500 μm (length). In addition to the five sets shown here, the other 30 additional sets (not shown) are used to analyze the effects of particle size, void size, particle content, and porosity.

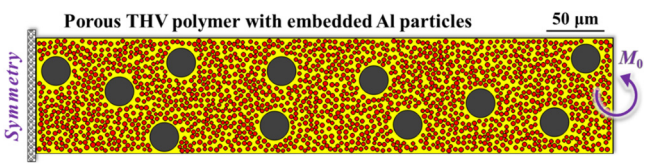

FIG. 3. A computational model showing the explicit consideration of Al particles (red) and voids (black) within THV polymer (yellow). The composite (MS No. 1 in Fig. 2 with 40% Al by weight and 10% porosity) is subjected to pure bending via external moment load (M_0). The upward deflection at the tip is Δ_0 = 50 μm.

Downloaded from http://pubs.aip.org/aip/jap/article-pdf/doi/10.1063/5.0141173/16966722/164101_1_5.0141173.pdf

Published under an exclusive license by AIP Publishing

TABLE I. Physical and electromechanical properties of the constituents.[28,51]

Material	ρ (kg/m^3)	ϵ/ϵ_0	E (MPa)	ν	μ_{TR}° (nC/m)
THV polymer	1980	4.47	22	0.4	5.12
Al particles	2702	…	70×10^3	0.33	…

$\varepsilon_{ij} = \frac{1}{2}(u_{i,j} + u_{j,i} + u_{k,i}u_{k,j})$, respectively; $\boldsymbol{\epsilon}$ and μ_{ijkl} are isotropic dielectric permittivity (absolute) and flexoelectric coefficient tensor, respectively. The electric field vector is given as $E_k = -\partial\varphi/\partial x_k$ with φ denoting the scalar electric potential. The value of $\boldsymbol{\epsilon}$ is given in Table I in terms of the vacuum permittivity ($\epsilon_0 = 8.854 \times 10^{-12}$ F/m).

The flexoelectric response is assumed to be isotropic, such that the fourth-order flexoelectric coefficient tensor can be fully determined using two independent constants,[49] similar to the isotropic linear elastic modulus tensor [see Eq. (6)]. Specifically,

$$\mu_{ijkl} = \mu_{TR}\left[\lambda\left(\delta_{ij}\delta_{kl} + \delta_{ik}\delta_{jl}\right) + \delta_{il}\delta_{jk}\right], \tag{3}$$

where $\mu_{TR} = \mu_{ijji}$ ($i, j = 1, 2, 3$; $i \neq j$; no summation implied for the repeated indices: i and j) denotes the transverse flexoelectric coefficient, whose value is listed in Table I; and $\lambda \equiv \mu_{SH}/\mu_{TR}$ is the ratio of the shear flexoelectric coefficient $\mu_{SH} = \mu_{iijj} = \mu_{ijij}$ ($i, j = 1, 2, 3$; $i \neq j$; no summation implied for the repeated indices) to the transverse flexoelectric coefficient μ_{TR}. The longitudinal coefficient is $\mu_{LT} = \mu_{iiii} = (1 + 2\lambda)\mu_{TR}$ ($i = 1, 2, 3$; no summation implied for the repeated index).

It is noted that the experimentally measured values of the flexoelectric properties of homogeneous materials (e.g., from cantilever beam bending) are often reported with the longitudinal strain gradient effect included,[1,3,4] owing to the coexistence of the lateral strain, which is proportional to the axial bending strain via Poisson's ratio. Assuming plane-strain conditions, this apparent transverse flexoelectric coefficient (μ_{TR}°) can be expressed as

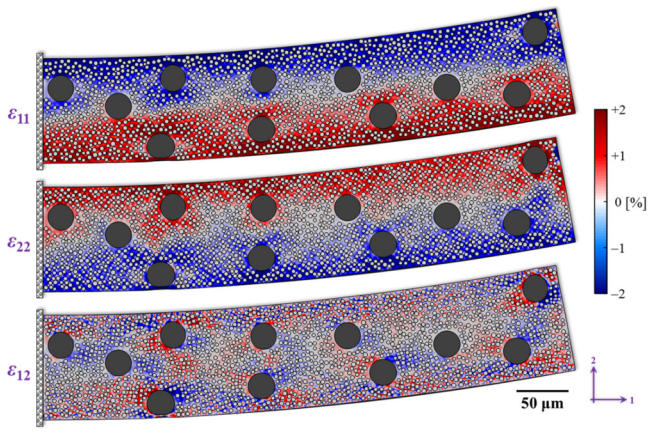

FIG. 4. Distributions of in-plane strain components for porous THV/Al (MS No. 1 shown here with 40% Al and 10% porosity, as in Fig. 3) under CBB with $\Delta_0 = 50\,\mu$m.

$\mu_{TR}^{\circ} = \mu_{TR} - \nu\mu_{LT}$. Furthermore, since it is difficult to measure μ_{SH} and μ_{LT} directly and no values are reported for them in the literature for THV, a parametric study is carried out systematically by varying the value of λ over a range to explore the trends and to determine μ_{SH} and μ_{LT} via best-fit to experimental data for the THV/Al composites. Here, it is found parametrically that $\lambda = -0.625$ yields the best comparison to the experimental results. The flexoelectric part of the polarization can be expressed as

$$P_i^{flexo} = \mu_{ijkl}\varepsilon_{jk,l} = \mu_{TR}(\varepsilon_{jj,i} + 2\lambda\varepsilon_{ij,j}). \tag{4}$$

The second Piola–Kirchhoff stress ($\boldsymbol{S}$) and the Green–Lagrange strain ($\boldsymbol{\varepsilon}$) are used to express the coupled electromechanical constitutive relation, which includes the effect of converse flexoelectricity[50] as

$$S_{ij} = JF_{ik}^{-1}C_{klmn}\varepsilon_{mn}F_{jl}^{-1} - \mu_{lijk}\frac{\partial E_l}{\partial x_k}, \tag{5}$$

where the elastic stiffness tensor can be expressed as

$$C_{ijkl} = \frac{\nu E}{(1+\nu)(1-2\nu)}\delta_{ij}\delta_{kl} + \frac{E}{2(1+\nu)}(\delta_{ik}\delta_{jl} + \delta_{il}\delta_{jk}), \tag{6}$$

with E and ν denoting Young's modulus and Poisson's ratio (see Table I), respectively.

III. RESULTS AND DISCUSSION

A. Electromechanical response at the microstructure level

To study how the microstructure's heterogeneities affect the effective flexoelectric behavior of the composite, the mechanical and electrical responses of the composite are analyzed. In Fig. 4, the two normal strains (ε_{11} and ε_{22}) and the in-plane shear strain ε_{12} are shown for a specimen (MS No. 1; 40% Al particles by weight and 10% porosity in Fig. 3). Here, the "1" direction is parallel to the beam's axis, while the "2" direction is perpendicular to the beam's axis.

When a positive moment is applied at the tip of the specimen as shown, the upper half of the beam experiences local compression along the axial direction, whereas the lower portion experiences tension. The magnitude of ε_{11} is relatively low along the centerline (i.e., near the neutral axis). The bending also induces a normal strain along the lateral direction (ε_{22}), as the specimen expands and contracts transversely in regions of flexural compression and tension, respectively, due to the Poisson effect. Moreover, the heterogeneity effect caused by the inclusions also engenders microscopic shear strains within the specimen. The focus of this analysis is on the direct flexoelectric effect. To gain a perspective on the scale of the converse flexoelectric effect, the axial stress (S_{11}) distribution is shown in Fig. 5. It can be seen that the magnitude of the part of the stress due to the converse flexoelectric effect [i.e., the last term shown in Eq. (5)] is negligible.

To gain further insight into the deformation, the individual strain gradient components are analyzed. Figure 6 delineates the gradients of the three in-plane strain components for the

Downloaded from http://pubs.aip.org/aip/jap/article-pdf/doi/10.1063/5.0141173/16966722/164101_1_5.0141173.pdf

Published under an exclusive license by AIP Publishing

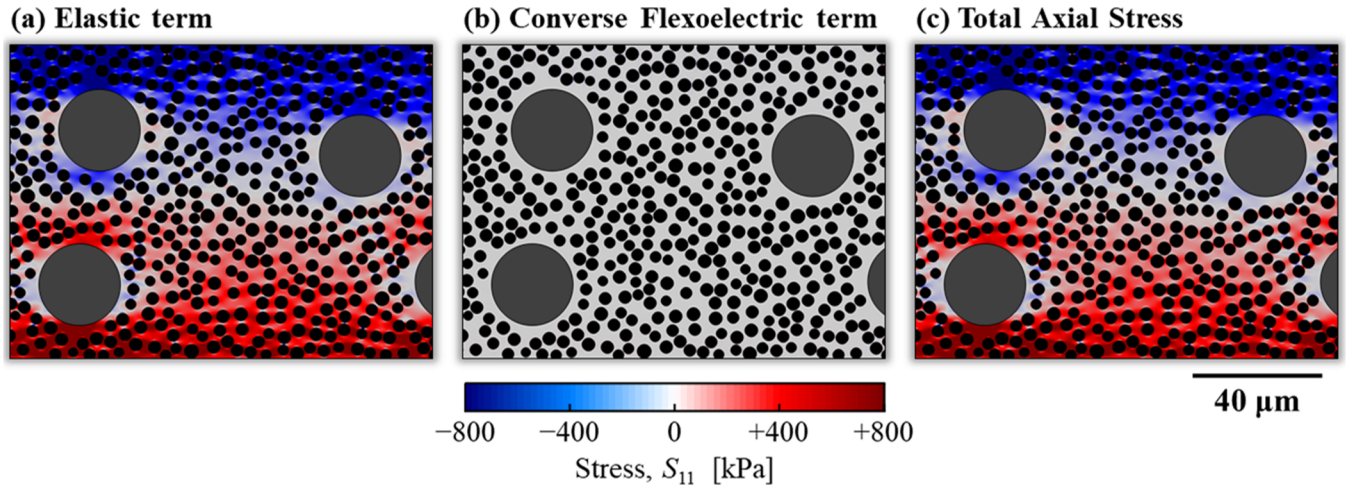

FIG. 5. Comparison of contributions to the second Piola–Kirchhoff stress S_{11}, (a) elastic contribution, (b) converse flexoelectric contribution, and (c) total. Results near the microstructural inclusions are shown for the microstructure in Fig. 3 and $\Delta_0 = 50\,\mu$m.

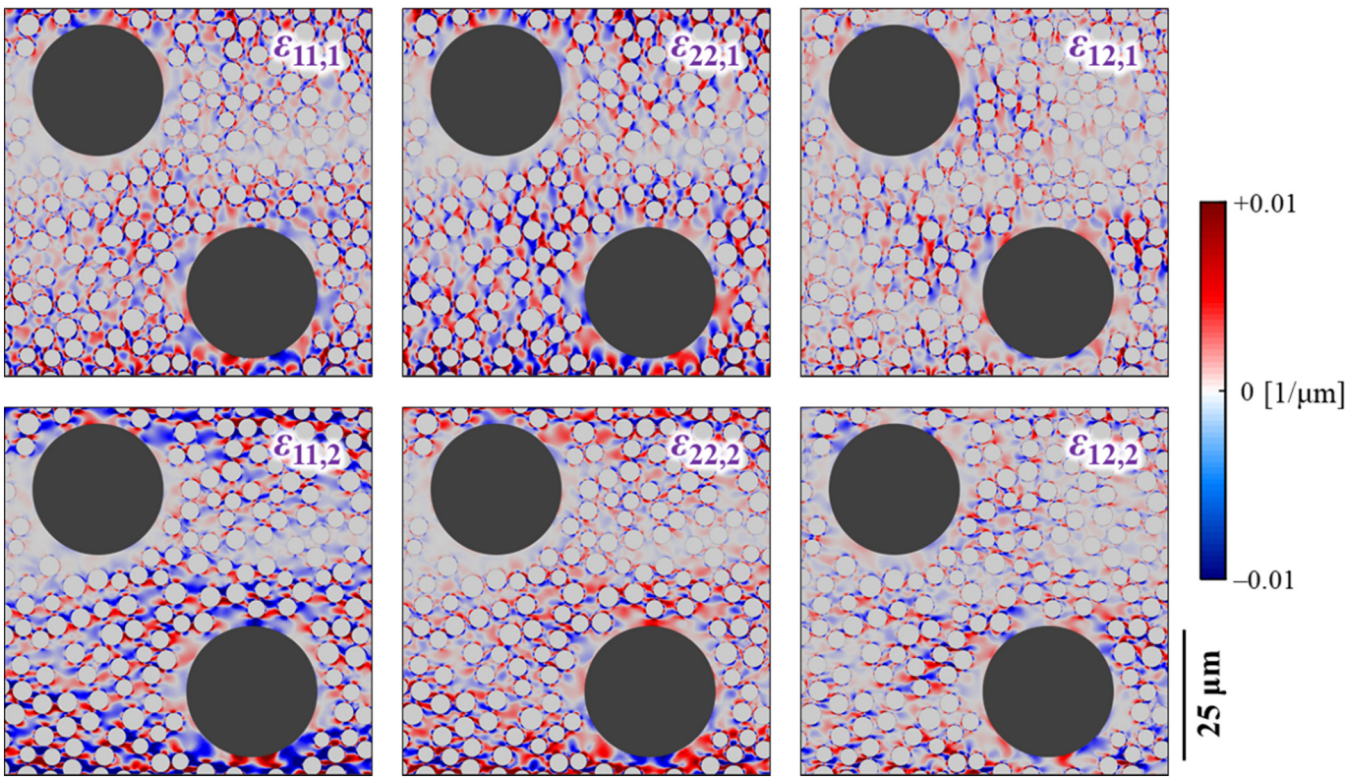

FIG. 6. Close-up view of the strain gradient components showing higher magnitudes near the particles and voids. The results are for the porous microstructure shown in Fig. 3 at $\Delta_0 = 50\,\mu$m.

Downloaded from http://pubs.aip.org/aip/jap/article-pdf/doi/10.1063/5.0141173/16966722/164101_1_5.0141173.pdf

Published under an exclusive license by AIP Publishing

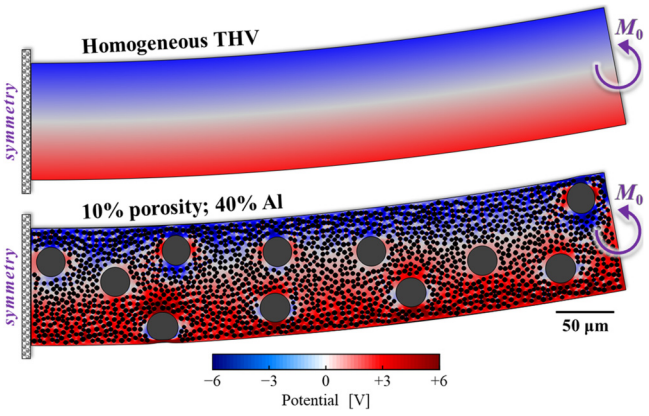

FIG. 7. Comparison of potential distributions between homogeneous (top) and inhomogeneous (bottom) specimens under CBB ($\Delta_0 = 50\,\mu$m). The microstructure for the inhomogeneous specimen is shown in Fig. 3.

microstructure shown in Fig. 3. Here, $\varepsilon_{11,1}$ and $\varepsilon_{22,2}$ are the longitudinal strain gradients; $\varepsilon_{11,2}$ and $\varepsilon_{22,1}$ are the transverse strain gradients; $\varepsilon_{12,1}$ and $\varepsilon_{12,2}$ are the shear strain gradients.

The stiffness mismatch among the various constituents promotes a significant enhancement of the local strain gradients near the particles and voids. The multidirectional state of strain gradient due to the introduction of Al particles and voids demonstrates that the effective flexoelectric behavior may be manipulated or tailored by controlling the size and level of the microstructural heterogeneities within a flexoelectric material. The effects of heterogeneities on the induced electrical output can be seen in Fig. 7, which

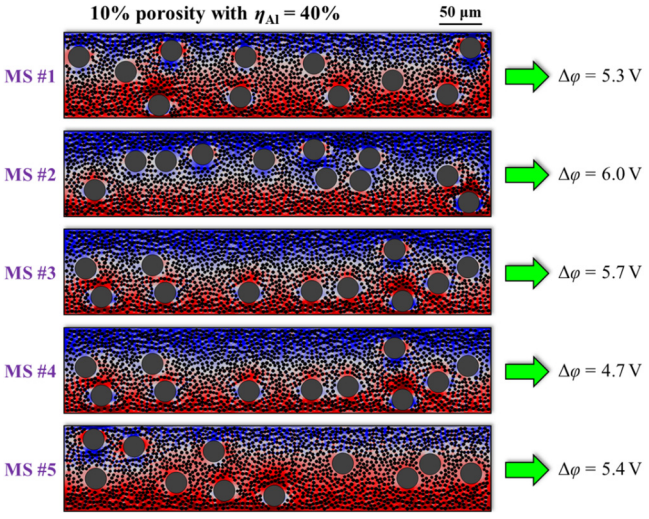

FIG. 8. Distributions of the electrical potential in the undeformed configurations of the five microstructures in the SEMSS with 10% porosity and 40% Al by weight shown in Fig. 2 ($\Delta_0 = 50\,\mu$m).

compares the electric potential distributions in a homogeneous THV and the inhomogeneous composite microstructure shown in Fig. 3. When subjected to the same magnitude of deformation ($\Delta_0 = 50\,\mu$m), the potential differences ($\Delta\varphi$) across the top and bottom surfaces are 5.5 and 5.3 V for the homogeneous and inhomogeneous specimens, respectively. In contrast to the uniformity seen in the potential field of the homogeneous specimen, the electrical response of the inhomogeneous specimen is profoundly influenced in the vicinity of the Al particles and voids, owing to both the localized magnification of the gradients of the normal strains (ε_{11} and ε_{22}) and the activation of the gradients of the shear strains (ε_{12} and ε_{21}), which are non-existent in the homogeneous case.

The electromechanical polarization in the microstructure is evaluated using Eq. (4). Integration of the polarization component in the "2" (vertical) direction over the entire microstructure yields the output potential between the top and bottom surfaces, which is what is measured in the experiments.[28] The electrical potential fields of the five microstructures in the SEMSS with 10% porosity and 40% of Al by weight are shown in Fig. 8. There is a degree of variation in both the local fields and the overall electrical outputs due to the stochastic nature of material heterogeneities. For example, the potential difference across the top and bottom surfaces varies between 4.7 and 6.0 V for the five specimens evaluated under ($\Delta_0 = 50\,\mu$m). The use of SEMSS allows for a more accurate and realistic characterization of the underlying behavioral trend and a systematic quantification of the behavioral fluctuations from specimen to specimen.

B. Macroscopic response

The effects of microstructural heterogeneities on the effective flexoelectric behavior of the composite are analyzed here. To assess the overall macroscopic response, the electric polarization across the top and bottom surfaces of each specimen is evaluated as

$$\bar{P}_2 = \frac{1}{\Omega}\int_{\Omega} P_2(\boldsymbol{x})\,dV = \bar{\mu}_{TR}\bar{\varepsilon}_{11,2}, \tag{7}$$

where the "overbar" symbol denotes the macroscopic effective or average value of the respective variable and Ω is the total volume of the specimen. This leads to the effective transverse flexoelectric coefficient ($\bar{\mu}_{TR}$) of the composite as

$$\bar{\mu}_{TR} = \frac{\mu_{TR}\int_{\Omega_b}[\varepsilon_{11,2} + 2\lambda\varepsilon_{12,1} + (1+2\lambda)\varepsilon_{22,2}]\,dV}{\int_{\Omega}\varepsilon_{11,2}\,dV}, \tag{8}$$

where Ω_b is the volume of the THV polymer (which is the only constituent that is flexoelectric) in the microstructure. Equation (8) shows that $\bar{\mu}_{TR}$ can be determined from the fields of the strain gradient components and the flexoelectric properties (i.e., μ_{TR} and λ) of the homogeneous THV polymer. The first term in the numerator corresponds to the flexoelectric polarization caused by the transverse strain gradient, while the second and third terms correspond to the polarizations caused by the shear and longitudinal strain gradients, respectively.

To study the effects of the microstructural heterogeneities on the macroscopic flexoelectricity of the THV/Al composite, a set of parametric analyses are performed. The flexoelectric coefficient

Downloaded from http://pubs.aip.org/aip/jap/article-pdf/doi/10.1063/5.0141173/16966722/164101_1_5.0141173.pdf

Published under an exclusive license by AIP Publishing

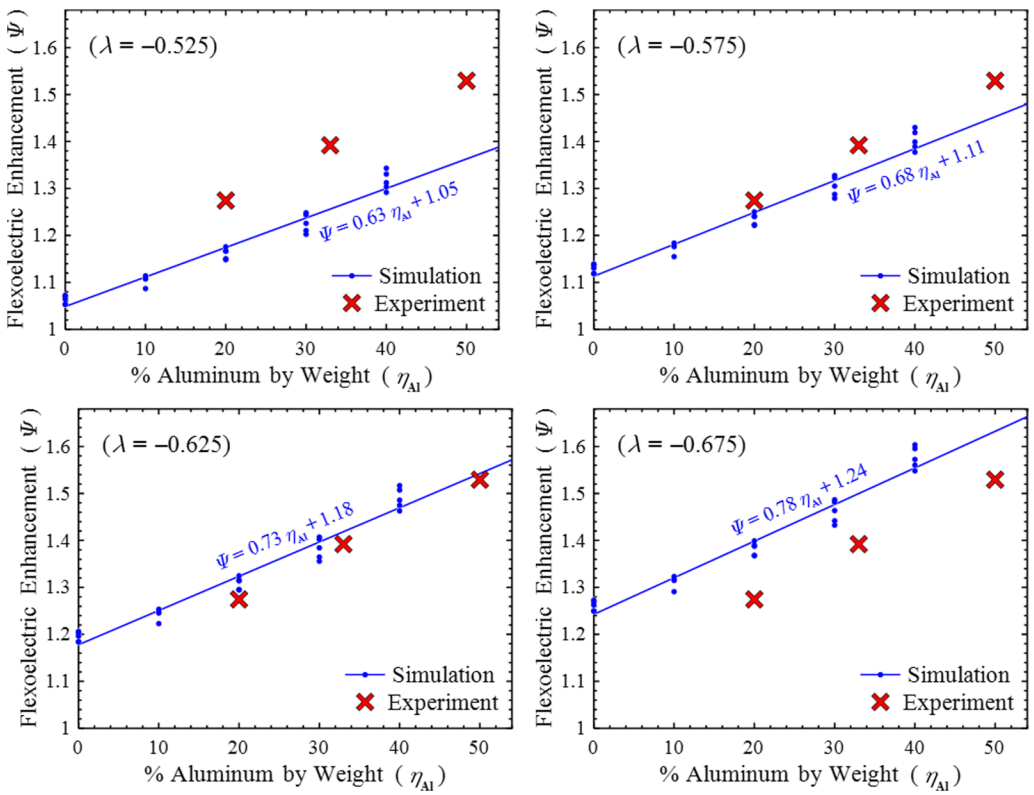

FIG. 9. Enhancement parameter (ψ) for the macroscopic transverse flexoelectric coefficient $\bar{\mu}_{TR}$ as a function of Al content (η_{Al}). The results for λ values between −0.525 and −0.675 are shown. Five statistically similar microstructures are used at each level of Al content. All specimens are 10% in porosity.

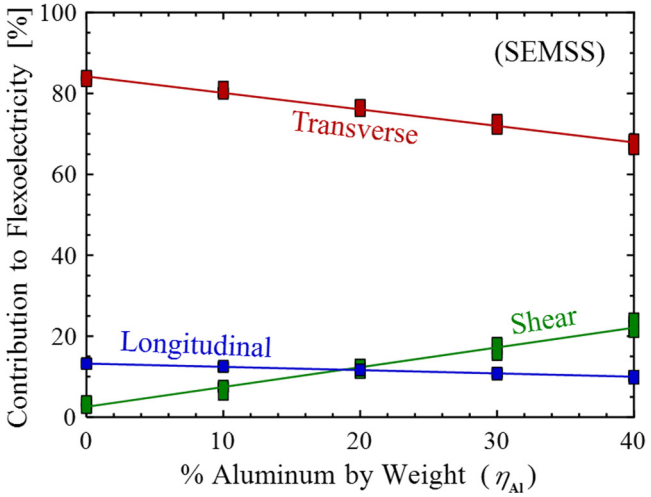

FIG. 10. Individual contributions to the macroscopic transverse flexoelectric coefficient for η_{Al} ranging between 0% and 40% wt. In all cases, porosity is 10% and λ is −0.625. The void size and mean particle size are 25 and 3.5 μm, respectively.

obtained from experiments[28] is used as a basis for calibration and comparison. The ratio between the effective flexoelectric coefficients of a heterogeneous composite and the homogeneous THV polymer under CBB ($\Psi \equiv \bar{\mu}_{TR}/\mu_{TR}$) is taken as a measure for the microstructure enhancement of the overall flexoelectric output. The results are shown in Fig. 9, which includes a parametric study.

The shear and longitudinal flexoelectric coefficients of THV are determined by varying the ratio $\lambda \equiv \mu_{SH}/\mu_{TR}$ for microstructures with 10% voids (the approximate porosity tested in the experiment) and Al particle fractions between 0% and 40%. The parametric study involves λ values between −0.525 and −0.675. The results suggest that $\lambda \equiv \mu_{SH}/\mu_{TR} = -0.625$ yields the best match, yielding $\mu_{SH} = -2.91$ nC/m and $\mu_{LT} = -1.16$ nC/m. In the analyses to follow, $\lambda = -0.625$ is used.

Figure 9 also shows the effect of Al content on the flexoelectric enhancement (Ψ). The effective flexoelectric coefficient of the composite $\bar{\mu}_{TR}$ increases monotonically with Al content, as the particles intensify the local strain gradients and activates the shear strain gradients, which do not occur in homogeneous specimens under CBB. For the specimen shown in Fig. 3, the flexoelectric enhancement is between 1.18 and 1.47 for Al content between 0% and 40%, leading to as much as ∼22% difference within this range.

Downloaded from http://pubs.aip.org/aip/jap/article-pdf/doi/10.1063/5.0141173/16966722/164101_1_5.0141173.pdf

Published under an exclusive license by AIP Publishing

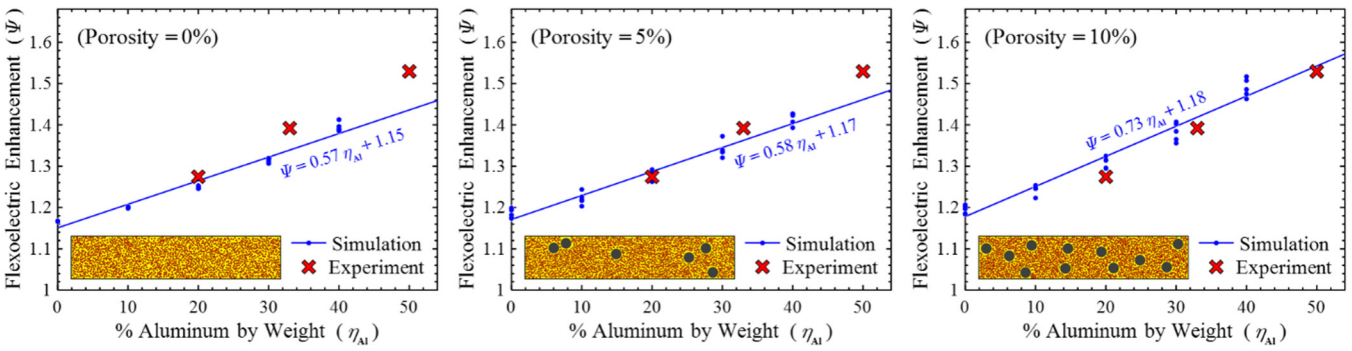

FIG. 11. Comparison of the transverse flexoelectric enhancement between THV/Al specimens with 0% (left), 5% (center), and 10% (right) porosity levels. All cases have a mean particle size of 3.5 μm. The void size assumed in the two porous cases is 25 μm. Five statistically similar microstructures are used for each material case.

The relative contributions of the three strain gradient terms to $\bar{\mu}_{TR}$ in Eq. (8) are plotted in Fig. 10 for the microstructure in Fig. 3. While the transverse term dominates, the shear and longitudinal terms also constitute significant contributions. While the contributions of the transverse and longitudinal terms decrease as the Al content increases, the contribution of the shear strain gradient term increases with the Al content. Because of this trend, at lower Al content levels (< 20%), the contribution to $\bar{\mu}_{TR}$ of the longitudinal strain gradient outweighs the contribution of the shear strain gradient, while at higher Al content levels (>20%), the shear strain gradient plays a more pivotal role than the longitudinal strain gradient. At an Al particle content of 40%, the contribution from the transverse term accounts for 67.4% of $\bar{\mu}_{TR}$, while those from the shear and longitudinal terms account for 22.7% and 9.9%, respectively.

C. Effects of particle content, porosity, particle size, and void size

In addition to the Al content, other effects of microstructure features are also explored. First, as shown in Fig. 11, the porosity effect is studied by comparing the flexoelectric enhancement for 0% (non-porous), 5%, and 10% porosity levels for microstructures with 0–40% wt. of Al. Here, a void size of 25 μm is used for the two sets of porous specimens. The flexoelectric enhancement (Ψ) is higher with voids than without voids. Specifically, Ψ at 10% voids is higher than at 0% voids by the following amounts: 2.4% at 0% Al and 6.3% at 40% Al. This increase in the effective flexoelectricity of porous specimens can be attributed to the increased magnitude of strain gradients near the voids.

The results in Fig. 12 illustrate how the Al particle size (D_{Al}) can affect the macroscopic flexoelectricity of the specimens. The comparison is made between non-porous microstructures with different particle sizes (3.5 μm, 7.0 μm and 10.5 μm in diameter) and Al content between 0% and 40% wt. Smaller Al particles generally lead to a higher effective flexoelectric output. The net difference between the 3.5 and 10.5 μm cases is 7.4% at 40% wt. Al. This trend is due to the fact that smaller particles cause the local strain gradient to be relatively higher near the particles.

Furthermore, Fig. 13 shows the effect of void size (D_{void}). The microstructures all have 10% porosity, 3.5 μm particle size in diameter, and Al content ranging between 0% and 40%. Compared to the trend exhibited by various Al particle sizes, varying the void

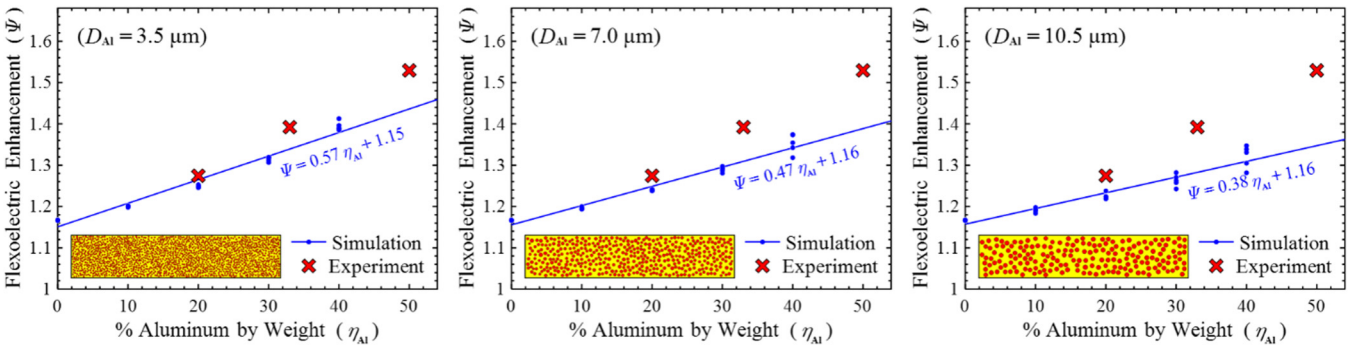

FIG. 12. Comparison of the transverse flexoelectric enhancement between THV/Al specimens with mean particle size of 3.5 μm (left), 7.0 μm (center), and 10.5 μm (right). All cases are non-porous. Five statistically similar microstructures are used for the material case.

Downloaded from http://pubs.aip.org/aip/jap/article-pdf/doi/10.1063/5.0141173/16966722/164101_1_5.0141173.pdf

Published under an exclusive license by AIP Publishing

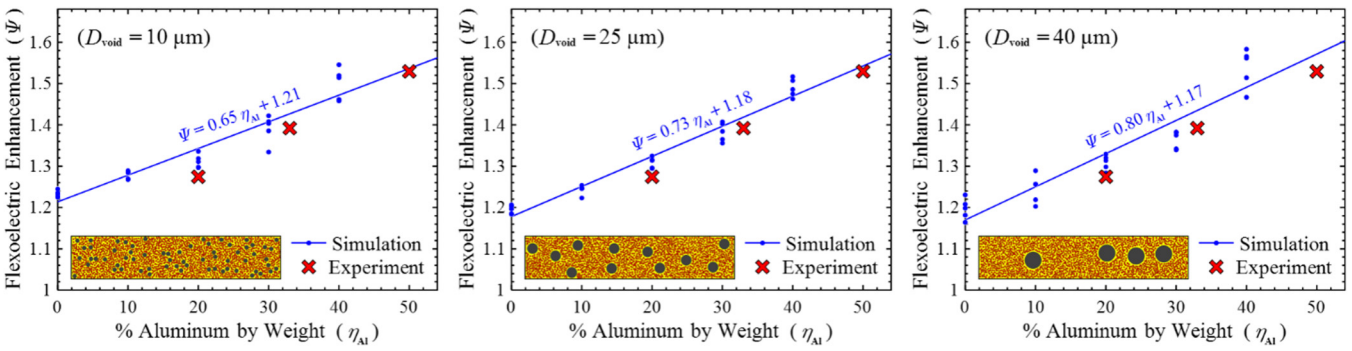

FIG. 13. Comparison of the transverse flexoelectric enhancement between THV/Al specimens with void size of 10 μm (left), 25 μm (middle), and 40 μm (right). All cases have a 10% porosity and a mean particle size of 3.5 μm. Five statistically similar microstructures are used for each material case.

size alone is shown to have relatively minor effect on the overall flexoelectric output. The net difference in the effective flexoelectric enhancement among the three sets of microstructures shown is limited to only 3.9% for the range of Al content analyzed.

Finally, the relationship between the macroscopic flexoelectric enhancement and the bulk stiffness of the inhomogeneous specimens is examined, as the enhancement depends not only on the degree of the relative size difference of the various constituents but also on the degree of the relative stiffness mismatch. Here, the bulk stiffness (i.e., effective Young's modulus) of the porous particulate composite is calculated using the Pal model (Model No. 2 listed under Table I).[52]

In Fig. 14, it can be seen that specimens with higher normalized effective modulus have higher flexoelectric enhancement for all microstructure cases shown. This is due to the role that stiffness mismatch has on intensifying the local strain gradient within the microstructure, thus enhancing the flexoelectric output at the macroscale.

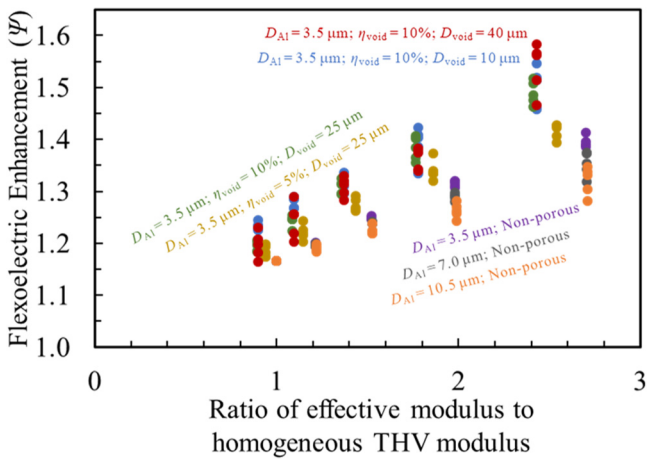

FIG. 14. Relationship between the macroscopic transverse flexoelectric enhancement and the normalized composite modulus for all 35 sets of the specimens examined.

IV. CONCLUSION

Microstructure can profoundly influence both the microscopic and macroscopic flexoelectric behavior of materials. To elucidate the influence of microstructural heterogeneities on the overall flexoelectric properties of THV/Al composites, an electromechanical computational model is developed to analyze the distributions of strain gradient and electrical polarization. Simulations are carried out using a cantilever beam bending (CBB) configuration, emulating companion experiments. The analyses allow the effective macroscopic transverse flexoelectric coefficient ($\bar{\mu}_{TR}$) to be systematically predicted as a function of microstructure attributes, including the contents and sizes of Al particles and voids. The results of the analyses closely track experimental results. It is found that both Al particles and voids markedly enhance the effective macroscopic flexoelectric coefficient. The enhancement comes from both the magnification of local longitudinal and transverse strain gradients relative to the homogeneous THV and the activation of shear strain gradients that are non-existent in homogenous materials under CBB.

The effective flexoelectric coefficient is shown to rise linearly with the level of Al particles in the material. At 40% Al content, the effective flexoelectric coefficient is ~22% higher than that homogenous THV without particles. A 10% porosity can cause the effective flexoelectric coefficient to be ~6.3% higher, compared to similar materials without voids. Overall, smaller microstructural heterogeneities, especially the Al particles, cause the local strain gradients to be higher, leading to higher flexoelectric output at the macroscale.

While the materials considered involve only particles and voids, the model and computational framework introduced herein can be applied to materials with other microstructural characteristics as well. For example, different metals with different electric and elastic properties can be used. Furthermore, dielectric particles with significantly different stiffness and dielectric constants from those of the polymer matrix can be used. Such changes may reveal new

Downloaded from http://pubs.aip.org/aip/jap/article-pdf/doi/10.1063/5.0141173/16966722/164101_1_5.0141173.pdf

Published under an exclusive license by AIP Publishing

regimes of behavior and offer avenues for tailoring the behavior of the composite. The approach and microstructure-flexoelectric behavior relations developed here can be utilized to carry out such analyses in the future and to design and engineer materials with desired electromechanical properties.

ACKNOWLEDGMENTS

This research was sponsored by the Air Force Office of Scientific Research Award Nos. FA9550-19-1-0008 and FA9550-19-1-0289 (Program Manager: Dr. Mitat Birkan). Any opinions, findings, conclusions, or recommendations expressed in the article are those of the authors and do not necessarily reflect the views of the U.S. Air Force.

AUTHOR DECLARATIONS

Conflict of Interest

The authors have no conflicts to disclose.

Author Contributions

Ju Hwan (Jay) Shin: Writing – original draft (lead); Writing – review & editing (lead). **Mikel J. Zaitzeff:** Writing – review & editing (supporting). **Lori J. Groven:** Writing – review & editing (supporting). **Min Zhou:** Funding acquisition (lead); Writing – original draft (equal); Writing – review & editing (lead).

DATA AVAILABILITY

The data that support the findings of this study are available from the corresponding author upon reasonable request.

REFERENCES

[1]S. Krichen and P. Sharma, "Flexoelectricity: A perspective on an unusual electromechanical coupling," J. Appl. Mech. **83**, 030801 (2016).
[2]A. Tagantsev, "Piezoelectricity and flexoelectricity in crystalline dielectrics," Phys. Rev. B **34**, 5883 (1986).
[3]P. Yudin and A. Tagantsev, "Fundamentals of flexoelectricity in solids," Nanotechnology **24**, 432001 (2013).
[4]P. Zubko, G. Catalan, and A. K. Tagantsev, "Flexoelectric effect in solids," Annu. Rev. Mater. Res. **43**, 387 (2013).
[5]S. Zhang, K. Liu, X. Wen, T. Wu, M. Xu, and S. Shen, "Converse flexoelectricity with relative permittivity gradient," Appl. Phys. Lett. **114**, 052903 (2019).
[6]Y. Gu, Z. Hong, J. Britson, and L. Q. Chen, "Nanoscale mechanical switching of ferroelectric polarization via flexoelectricity," Appl. Phys. Lett. **106**, 022904 (2015).
[7]E. Guo, R. Roth, S. Das, and K. Dörr, "Strain induced low mechanical switching force in ultrathin $PbZr_{0.2}Ti_{0.8}O_3$ films," Appl. Phys. Lett. **105**, 012903 (2014).
[8]S. Hu, H. Li, and H. Tzou, "Comparison of flexoelectric and piezoelectric dynamic signal responses on flexible rings," J. Intell. Mater. Syst. Struct. **25**, 832 (2014).
[9]W. Huang, X. Yan, S. R. Kwon, S. Zhang, F. G. Yuan, and X. Jiang, "Flexoelectric strain gradient detection using $Ba_{0.64}Sr_{0.36}TiO_3$ for sensing," Appl. Phys. Lett. **101**, 252903 (2012).
[10]S. R. Kwon, W. Huang, S. Zhang, F. G. Yuan, and X. Jiang, "Flexoelectric sensing using a multilayered barium strontium titanate structure," Smart Mater. Struct. **22**, 115017 (2013).
[11]H. Lu, C. W. Bark, D. Esque De Los Ojos, J. Alcala, C. B. Eom, G. Catalan, and A. Gruverman, "Mechanical writing of ferroelectric polarization," Science **336**, 59 (2012).
[12]Z. Wen, X. Qiu, C. Li, C. Zheng, X. Ge, A. Li, and D. Wu, "Mechanical switching of ferroelectric polarization in ultrathin $BaTiO_3$ films: The effects of epitaxial strain," Appl. Phys. Lett. **104**, 042907 (2014).
[13]X. Yan, W. Huang, S. R. Kwon, S. Yang, X. Jiang, and F. G. Yuan, "A sensor for the direct measurement of curvature based on flexoelectricity," Smart Mater. Struct. **22**, 085016 (2013).
[14]S. Zhang, K. Liu, M. Xu, and S. Shen, "A curved resonant flexoelectric actuator," Appl. Phys. Lett. **111**, 082904 (2017).
[15]S. Zhang, M. Xu, K. Liu, and S. Shen, "A flexoelectricity effect-based sensor for direct torque measurement," J. Phys. D: Appl. Phys. **48**, 485502 (2015).
[16]W. Zhou, P. Chen, Q. Pan, X. Zhang, and B. Chu, "Lead-free metamaterials with enormous apparent piezoelectric response," Adv. Mater. **27**, 6349 (2015).
[17]X. Jiang, W. Huang, and S. Zhang, "Flexoelectric nano-generator: Materials, structures and devices," Nano Energy **2**, 1079 (2013).
[18]J. X. Chen, J. W. Li, C. C. Cheng, and C. W. Chiu, "Piezoelectric property enhancement of PZT/poly(vinylidenefluoride-co-trifluoroethylene) hybrid films for flexible piezoelectric energy harvesters," ACS Omega **7**, 793 (2022).
[19]J. W. Li, C. Y. Huang, K. Y. Chen, J. X. Chen, X. Y. Hsu, Y. F. Chen, C. F. J. Kuo, C. C. Cheng, M. C. Suen, and C. W. Chiu, "Enhanced piezoelectric properties of poly(vinylidenefluoride-co-trifluoroethylene)/carbon-based nanomaterial composite films for pressure sensing applications," Polymers **12**, 2999 (2020).
[20]T. Zheng, H. Wu, Y. Yuan, X. Lv, Q. Li, T. Men, C. Zhao, D. Xiao, J. Wu, and K. Wang, "The structural origin of enhanced piezoelectric performance and stability in lead free ceramics," Energy Environ. Sci. **10**, 528 (2017).
[21]H. Wu, Y. Zhang, J. Wu, J. Wang, and S. J. Pennycook, "Microstructural origins of high piezoelectric performance: A pathway to practical lead-free materials," Adv. Funct. Mater. **29**, 1902911 (2019).
[22]J. Wu, *Advances in Lead-Free Piezoelectric Materials* (Springer, 2018).
[23]H. Su, X. Wang, C. Li, Z. Wang, Y. Wu, J. Zhang, Y. Zhang, C. Zhao, J. Wu, and H. Zheng, "Enhanced energy harvesting ability of polydimethylsiloxane-$BaTiO_3$-based flexible piezoelectric nanogenerator for tactile imitation application," Nano Energy **83**, 105809 (2021).
[24]J. Narvaez, F. Vasquez-Sancho, and G. Catalan, "Enhanced flexoelectric-like response in oxide semiconductors," Nature **538**, 219 (2016).
[25]U. K. Bhaskar, N. Banerjee, A. Abdollahi, Z. Wang, D. G. Schlom, G. Rijnders, and G. Catalan, "A flexoelectric microelectromechanical system on silicon," Nat. Nanotechnol. **11**, 263 (2016).
[26]L. Shu, S. Ke, L. Fei, W. Huang, Z. Wang, J. Gong, X. Jiang, L. Wang, F. Li, and S. Lei, "Photoflexoelectric effect in halide perovskites," Nat. Mater. **19**, 605 (2020).
[27]J. H. Shin, D. K. Messer, M. Örnek, S. F. Son, and M. Zhou, "Dielectric breakdown driven by flexoelectric and piezoelectric charge generation as hotspot ignition mechanism in aluminized fluoropolymer films," J. Appl. Phys. **132**, 085101 (2022).
[28]M. J. Zaitzeff and L. J. Groven, "Flexoelectricity in fluoropolymer/aluminum reactives," Polym. Int. **71**, 829 (2022).
[29]L. Shu, Z. Yong, X. Jiang, Z. Xie, and W. Huang, "Flexoelectricity in low densification materials and its implication," J. Alloys Compd. **695**, 1555 (2017).
[30]D. Yan, J. Wang, J. Xiang, Y. Xing, and L. H. Shao, "A flexoelectricity-enabled ultrahigh piezoelectric effect of a polymeric composite foam as a strain-gradient electric generator," Sci. Adv. **9**, eadc8845 (2023).
[31]A. E. Giannakopoulos and A. J. Rosakis, "Dynamics of flexoelectric materials: Subsonic, intersonic, and supersonic ruptures and Mach cone formation," J. Appl. Mech. **87**, 061004 (2020).
[32]D. K. Messer, J. H. Shin, M. Örnek, T. A. Hafner, M. Zhou, and S. F. Son, "Effects of flexoelectric and piezoelectric properties on the impact-driven ignition sensitivity of P(VDF-TrFE)/nAl films," Combust. Flame **242**, 112181 (2022).
[33]J. H. Shin and M. Zhou, "Piezoelectric response of energetic composites under an electrostatic excitation," J. Appl. Phys. **129**, 245103 (2021).

Downloaded from http://pubs.aip.org/aip/jap/article-pdf/doi/10.1063/5.0141173/16966722/164101_1_5.0141173.pdf

Published under an exclusive license by AIP Publishing

[34]S. L. Row and L. J. Groven, "Smart energetics: Sensitization of the aluminum-fluoropolymer reactive system," Adv. Eng. Mater. **20**, 1700409 (2018).
[35]M. Örnek, K. E. Uhlenhake, Y. Zhou, B. Zhang, M. Kalaswad, D. N. Collard, H. Wang, Q. Wang, and S. F. Son, "Preparation and characterization of multi-functional piezoenergetic polyvinylidene fluoride/aluminum nanocomposite films," J. Appl. Phys. **131**, 055108 (2022).
[36]Y. Liu and Q. Wang, "Ferroelectric polymers exhibiting negative longitudinal piezoelectric coefficient: Progress and prospects," Adv. Sci. **7**, 1902468 (2020).
[37]X. Hu, Y. Zhou, J. Liu, and B. Chu, "Improved flexoelectricity in PVDF/barium strontium titanate (BST) nanocomposites," J. Appl. Phys. **123**, 154101 (2018).
[38]B. Ploss, W. Y. Ng, H. L. W. Chan, B. Ploss, and C. L. Choy, "Poling study of PZT/P(VDF–TrFE) composites," Compos. Sci. Technol. **61**, 957 (2001).
[39]D. Q. Zhang, D. W. Wang, J. Yuan, Q. L. Zhao, Z. Y. Wang, and M. S. Cao, "Structural and electrical properties of PZT/PVDF piezoelectric nanocomposites prepared by cold-press and hot-press routes," Chin. Phys. Lett. **25**, 4410 (2008).
[40]T. Yamada, T. Ueda, and T. Kitayama, "Piezoelectricity of a high-content lead zirconate titanate/polymer composite," J. Appl. Phys. **53**, 4328 (1982).
[41]D. Waller, T. Iqbal, and A. Safari, "Poling of lead zirconate titanate ceramics and flexible piezoelectric composites by the corona discharge technique," J. Am. Ceram. Soc. **72**, 322 (1989).
[42]D. Chen, T. Sharma, and J. X. Zhang, "Mesoporous surface control of PVDF thin films for enhanced piezoelectric energy generation," Sens. Actuators A **216**, 196 (2014).
[43]M. Zhang, D. Yan, J. Wang, and L. H. Shao, "Ultrahigh flexoelectric effect of 3D interconnected porous polymers: Modelling and verification," J. Mech. Phys. Solids **151**, 104396 (2021).
[44]X. Zhao, S. Zheng, and Z. Li, "Effects of porosity and flexoelectricity on static bending and free vibration of AFG piezoelectric nanobeams," Thin Wall. Struct. **151**, 106754 (2020).
[45]Y. Zhou, J. Liu, X. Hu, B. Chu, S. Chen, and D. Salem, "Flexoelectric effect in PVDF-based polymers," IEEE Trans. Dielectr. Electr. Insul. **24**, 727 (2017).
[46]W. Ma and L. E. Cross, "Flexoelectric effect in ceramic lead zirconate titanate," Appl. Phys. Lett. **86**, 072905 (2005).
[47]A. Abdollahi, C. Peco, D. Millan, M. Arroyo, and I. Arias, "Computational evaluation of the flexoelectric effect in dielectric solids," J. Appl. Phys. **116**, 093502 (2014).
[48]J. Yang, *An Introduction to the Theory of Piezoelectricity Springer Science+Business Media* (Springer, 2005), Vol. 9.
[49]L. Shu, X. Wei, T. Pang, X. Yao, and C. Wang, "Symmetry of flexoelectric coefficients in crystalline medium," J. Appl. Phys. **110**, 104106 (2011).
[50]L. Shu, F. Li, W. Huang, X. Wei, X. Yao, and X. Jiang, "Relationship between direct and converse flexoelectric coefficients," J. Appl. Phys. **116**, 144105 (2014).
[51]H. Chalal and F. Abed-Meraim, "Hardening effects on strain localization predictions in porous ductile materials using the bifurcation approach," Mech. Mater. **91**, 152 (2015).
[52]R. Pal, "New models for effective Young's modulus of particulate composites," Compos. B: Eng. **36**, 513 (2005).

Downloaded from http://pubs.aip.org/aip/jap/article-pdf/doi/10.1063/5.0141173/16966722/164101_1_5.0141173.pdf

Published under an exclusive license by AIP Publishing